ACS APPLIED MATERIALS & INTERFACES

Research Article

www.acsami.org

Design of Two-Dimensional, Ultrathin MoS_2 Nanoplates Fabricated Within One-Dimensional Carbon Nanofibers With Thermosensitive Morphology: High-Performance Electrocatalysts For The Hydrogen Evolution Reaction

Han Zhu,[†] FengLei Lyu,[§] MingLiang Du,*[,†,‡] Ming Zhang,[†,‡] QingFa Wang,[§] JuMing Yao,[†,‡] and BaoChun Guo[∥]

[†]Department of Materials Engineering, College of Materials and Textile, Zhejiang Sci-Tech University, Hangzhou 310018, People's Republic of China

[‡]Key Laboratory of Advanced Textile Materials and Manufacturing Technology of the Ministry of Education, Zhejiang Sci-Tech University, Hangzhou 310018, People's Republic of China

[§]Key Laboratory for Green Chemical Technology of the Ministry of Education, School of Chemical Engineering and Technology, Tianjin University, 92 Weijin Road, Tianjin 300072, People's Republic of China

[∥]Department of Polymer Materials and Engineering, South China University of Technology, Guangzhou 510640, People's Republic of China

Supporting Information

ABSTRACT: Two-dimensional MoS_2 nanoplates within carbon nanofibers (CNFs) with monolayer thickness, nanometer-scale dimensions and abundant edges are fabricated. This strategy provides a well-defined pathway for the precise design of MoS_2 nanomaterials, offering control over the evolution of MoS_2 morphology from nanoparticles to nanoplates as well as from mono- to several-layer structures, over a lateral dimension range of 5 to 70 nm. CNFs play an important role in confining the growth of MoS_2 nanoplates, leading to increases in the amount of exposed edge sites while hindering the stacking and aggregation of MoS_2 layers, and accelerating electron transfer. The controlled growth of MoS_2 nanoplates embedded in CNFs is leveraged to demonstrate structure-dependent catalytic activity in the hydrogen evolution reaction (HER). The results suggest that increases in the number of layers and the lateral dimension result in a decrease in HER activity as a general rule. Single-layer MoS_2 nanoplates with abundant edges and a lateral dimension of 7.3 nm demonstrated the lowest hydrogen evolution reaction overpotential of 93 mV (J = 10 mA/cm^2), the highest current density of 80.3 mA/cm^2 at η = 300 mV and the smallest Tafel slope of 42 mV/decade. The ability of MoS_2−CNFs hybrids to act as nonprecious metal catalysts indicates their promise for use in energy-related electrocatalytic applications.

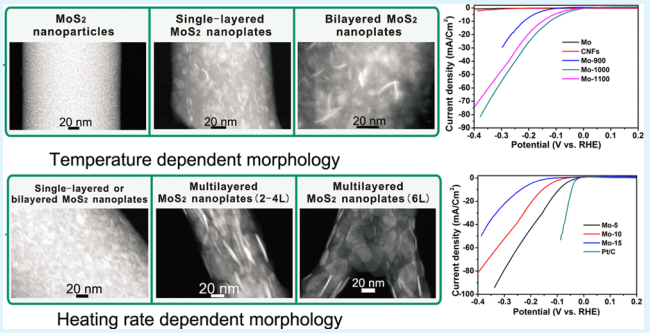

KEYWORDS: *two-dimensional, carbon nanofibers, electrocatalysis, hydrogen evolution, MoS_2*

INTRODUCTION

The construction of a hydrogen-based energy system has been repeatedly proposed as a solution to the severe global energy shortage and accompanying environmental deterioration, as hydrogen shows promise as an efficient, clean, and durable energy carrier.[1,2] Hydrogen may be evolved from the reduction of protons to form hydrogen gas, which is the reductive half-reaction of the splitting of water molecules.[3] This process usually requires the use of high-performance hydrogen evolution reaction (HER) electrocatalysts.[4−6] Although the platinum group metals have traditionally been the highest-performance catalysts for HER, these elements are rare and costly. Therefore, there is an ongoing search for earth-abundant, Pt-free catalysts in order to avoid the use of precious metals.[7,8] The abilities of a variety of non-noble materials to catalyze HER have been investigated, including those of transition metal alloys,[9] chalcogenides,[10−14] carbides,[15−17] nitrides,[18] and phosphides.[19] Despite extensive research, however, only a few synthetic catalysts have been found which can operate in water and yield high current densities at low overpotentials (η) and with quantitative current efficiencies.[3]

Among these alternatives, significant attention has been devoted to molybdenum disulfide (MoS_2), which demonstrates

Received: August 18, 2014
Accepted: November 24, 2014
Published: November 24, 2014

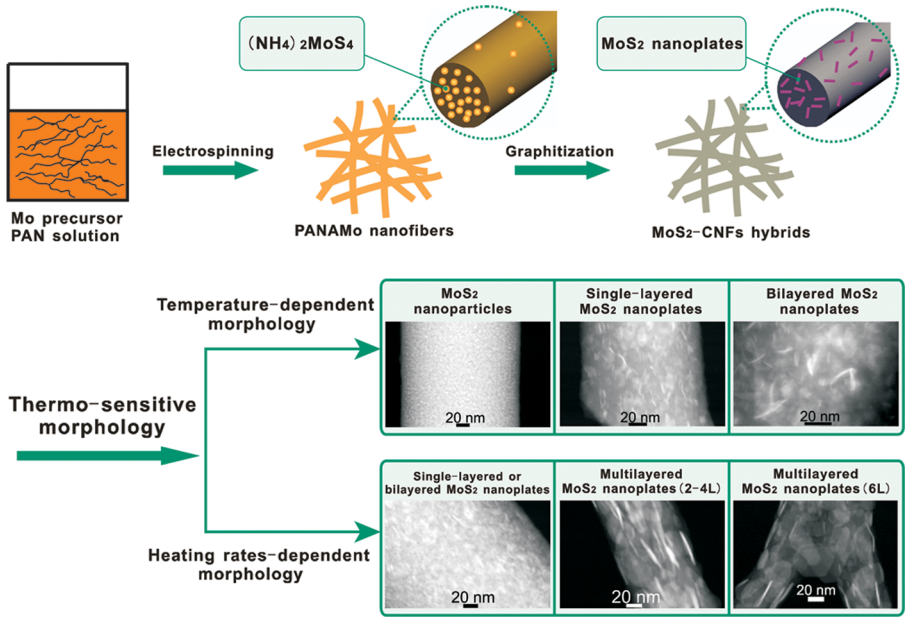

Figure 1. Schematic illustration of the synthesis procedure used to prepare MoS_2-carbon hybrid nanofibers and the thermosensitive morphology evolutions.

appealing levels of HER activity as well as being abundantly available. This research has led to the development of several different MoS_2-based HER electrocatalysts, in both crystalline[20−22] and amorphous[23−25] states. MoS_2 is a notable two-dimensional nanomaterial and has been widely used as a functional material in diverse applications, such as electronic transistors,[26] batteries,[27,28] photovoltaics,[29] and catalysis.[30−32] The chemical peculiarities of MoS_2 lead to unique mechanical, optical, and electrical properties. Two-dimensional MoS_2 sheets are formed of vertically stacked S−Mo−S interlayers. Results from both theoretical and experimental studies have demonstrated that catalytically active sites are situated on sulfided Mo edges, while the basal plane is inert. Several parameters, including the conductivity and roughness of the material, the abundance of active edge sites, and the means of attachment of the catalyst to the electrodes, must be tightly optimized to produce more active electrocatalysts.[2] However, layered MoS_2 crystals have a natural tendency to form closed structures such as fullerenes and nanotubes or stacked multilayered geometries, resulting in limited edge densities.[4]

Several methods have been attempted to produce single-layer or several-layer MoS_2, including mechanical exfoliation,[34] chemical exfoliation,[31,35] hydrothermal synthesis,[20,21] and chemical vapor deposition.[26,33] Exfoliated MoS_2 nanosheets are metastable, tetragonal monolayers (1T-MoS_2) possessing excellent HER activity. However, these materials display a strong tendency toward restacking and undergoing an irreversible phase transition to hexagonal 2H-MoS_2,[2,36] resulting in significant deterioration of the electrochemical performance. Moreover, the single-layer MoS_2 nanosheets that have been produced thus far have large aspect ratios. If a reduction in the lateral dimension was to be accomplished, novel properties may arise due to edge or quantum confinement effects.[4,37] However, developing an effective method to produce single-layer MoS_2 nanoplates with nanoscale lateral dimensions and greater amounts of edges exposure has remained a challenge.

Additionally, although nanosized MoS_2 may serve as a highly active electrocatalyst for HER due to the high exposure of numerous reactive sulfur edge sites, it is also a semiconductor with poor bulk conductivity and anisotropic electrical transport properties that limit catalytic efficiency.[4,5,31] This drawback may be addressed through the preparation of single-layer MoS_2 nanoplate-based composite materials, with partner materials that are conductive and easily percolating. In particular, nanoplates may be blended with carbonaceous materials. Recently, MoS_2-carbon composites have been found to be effective at enhancing both electron and mass transport.[2,31] Combining carbon nanotubes,[38] graphene,[39] or conductive polymers[40] with MoS_2 has also been shown to be effective in this respect. Their abundance, tunable molecular structures, and stability in both acidic and alkaline environments, are unique advantages possessed by carbon-based materials when designing catalysis. However, direct modification of MoS_2 with carbon results in an inability to balance between exposure of active sites and conductivity, and the number of layers and lateral dimensions of the nanosheets were found to be uncontrollable, thereby limiting the applicability of this approach.

The confinement of nanoparticles within conductive carbon materials, such as fullerenes, carbon nanotubes, or graphene has been proven to be effective in restricting the size of these particles to the nanometer scale, leading to improvements in their catalytic properties.[38,39] Recent results from our group describing the design of a system combining noble metal nanoparticles with carbon nanofibers revealed that small, uniform nanoparticles could be obtained easily using this combination due to the confinement of nanoparticle growth, resulting in both high catalytic activity and high stability.[41] Electrospun carbon nanofibers (CNFs) have been widely used in energy conversion and storage applications as this material is highly conductive and stable as well as having a large electrochemical surface area, making it an ideal carrier for MoS_2 nanocrystals. In addition, CNFs can serve as a host to confine the growth of MoS_2 nanoplates.

Herein, a novel and effective strategy is described for the synthesis of two-dimensional MoS_2 nanoplates with monolayer thickness, nanometer-scale dimensions, and abundant edges fabricated within one-dimensional CNFs. This scheme provides a well-defined pathway to enable precise design of morphological control over evolution both from nanoparticles to nanoplates and from mono- to several-layers, as well as control of the lateral dimension between 5 to 70 nm. CNFs play an important role in confining the growth of MoS_2 nanoplates by increasing the exposure of edge sites, hindering the stacking and aggregation of MoS_2 layers, and accelerating electron transfer. In the process introduced here, $(NH_4)_2MoS_4$ is dissolved in polyacrylonitrile (PAN) solution and then electrospun into continuous PAN-$(NH_4)_2MoS_4$ (PANAMo) nanofibers. After high-temperature treatment to promote the conversion of amorphous PAN nanofibers into graphene-layered CNFs, the $(NH_4)_2MoS_4$ starting material decomposes into MoS_2, forming MoS_2−CNFs hybrid nanomaterials. MoS_2 nanocrystals exhibit thermosensitive morphologies: increased graphitization temperatures and heating rates led to increases in the lateral dimension (from 7 to 70 nm) and number of layers (from 1 to 6), along with a phase transition from 1T MoS_2 to 2H MoS_2. The synthesis procedure and thermosensitive evolution of the morphology are illustrated in Figure 1. The controlled growth of MoS_2 nanoplates embedded in CNFs is used to demonstrate structure-dependent catalytic activity in the hydrogen evolution reaction. Single-layer MoS_2 nanoplates with abundant edges and a lateral dimension of 7.3 nm demonstrated the lowest HER overpotential, at 93 mV (J = 10 mA/cm^2); the highest current density, 80.3 mA/cm^2 at η = 300 mV; the smallest Tafel slope, 42 mV/decade. These metrics are close to those demonstrated by commercial Pt/C catalysts. The results suggest the general rule that increases in the number of layers and the lateral dimension result in a decrease in HER activity. The ability of MoS_2−CNFs hybrids to act as nonprecious metal catalysts indicates their promise for use in energy-related electrocatalytic applications.

RESULTS AND DISCUSSION

The thermolysis of $(NH_4)_2MoS_4$ under an inert environment has two overall steps, as described in the literature.[42] At low temperatures, between 120 and 360 °C, $(NH_4)_2MoS_4$ is converted to MoS_3 (eq 1). The second step, conversion from MoS_3 to MoS_2 (eq 2), requires annealing at a higher temperature, at least above 800 °C.[42]

$$(NH_4)_2MoS_4 \rightarrow 2NH_3 + H_2S + MoS_3 \quad (1)$$

$$MoS_3 \rightarrow MoS_2 + S \quad (2)$$

Typically, the PANAMo nanofibers produced using this method have a $(NH_4)_2MoS_4$ mass fraction of 12% and an average diameter of 560 nm. Images of the fibers (Figure 2a) reveal a distinct, random arrangement of nanofiber architectures. After graphitization treatment at 1000 °C, MoS_2−CNFs nanofibers are uniform and continuous, forming a 3D network (Figure 2b). The average diameter of MoS_2−CNFs is 220 nm, indicating that the fibers experience significant shrinkage during the graphitization process. Figure 2c shows the amorphous structure and uneven, rough surfaces of the PANAMo nanofibers. By contrast, the surfaces of MoS_2−CNFs samples (Figure 2d) are smooth, with thin MoS_2 nanoplates visibly embedded in a random distribution in the CNFs, demonstrating that the graphitization treatment was able to cause the formation of MoS_2 nanocrystals.

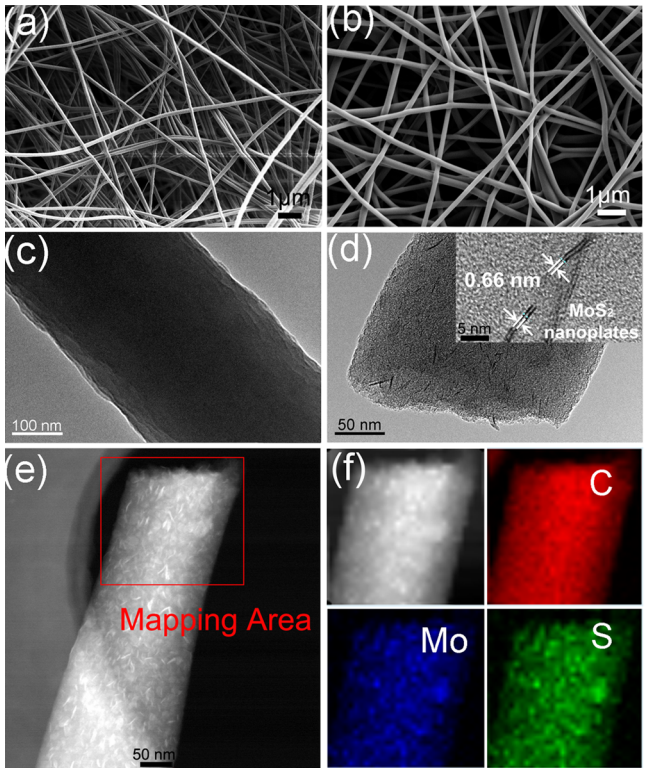

Figure 2. Field emission scanning electron microscopy (FE-SEM) and transmission electron microscopy (TEM) images of the (a, c) as-prepared PANAMo and (b, d) MoS_2−CNFs nanofibers treated at 1000 °C and 2 °C/min. Inset in panel d is a high resolution (HR)TEM image of the MoS_2−CNFs. (e) High angle annular dark field scanning transmission electron microscopy (HAADF-STEM) images of the MoS_2−CNFs and (f) STEM-EDS (energy-dispersive X-ray spectroscopy) mapping image of the selected area: C (red), Mo (dark blue), and S (green) elements.

The majority of the small MoS_2 nanoplates formed during graphitization exhibit two-layered structures, with an interlayer distance of 0.66 nm in the (002) plane and lateral dimensions ranging from 4 to 10 nm, as can be clearly seen using high resolution transmission electron microscopy (HRTEM) image (inset in Figure 2d). High angle annular dark field scanning transmission electron microscopy (HAADF-STEM) (Figure 2e) shows that the MoS_2 nanoplates are evenly dispersed throughout the CNF matrix. The edges of the MoS_2 nanoplates are also visible as pale white lines. These locations of these edges are consistent with the black lines seen in the transmission electron microscopy (TEM) images of MoS_2−CNFs (Figure 2d). The elemental composition of the MoS_2−CNFs was analyzed using scanning transmission electron microscopy energy-dispersive X-ray spectroscopy (STEM-EDS) mapping. The carbon content detected is due to the CNFs while the molybdenum and sulfur indicate the presence of MoS_2. The distribution of the detected elements is consistent with successful formation of embedded MoS_2 nanoplates in CNFs.

X-ray diffraction (XRD) analysis of PANAMo, pure CNF, and MoS_2−CNF samples was used to reveal more detail concerning the evolutions undergone by both the crystal and chemical structures of the materials during the graphitization process. As shown in Figure 3A, the nanofibrous mats of

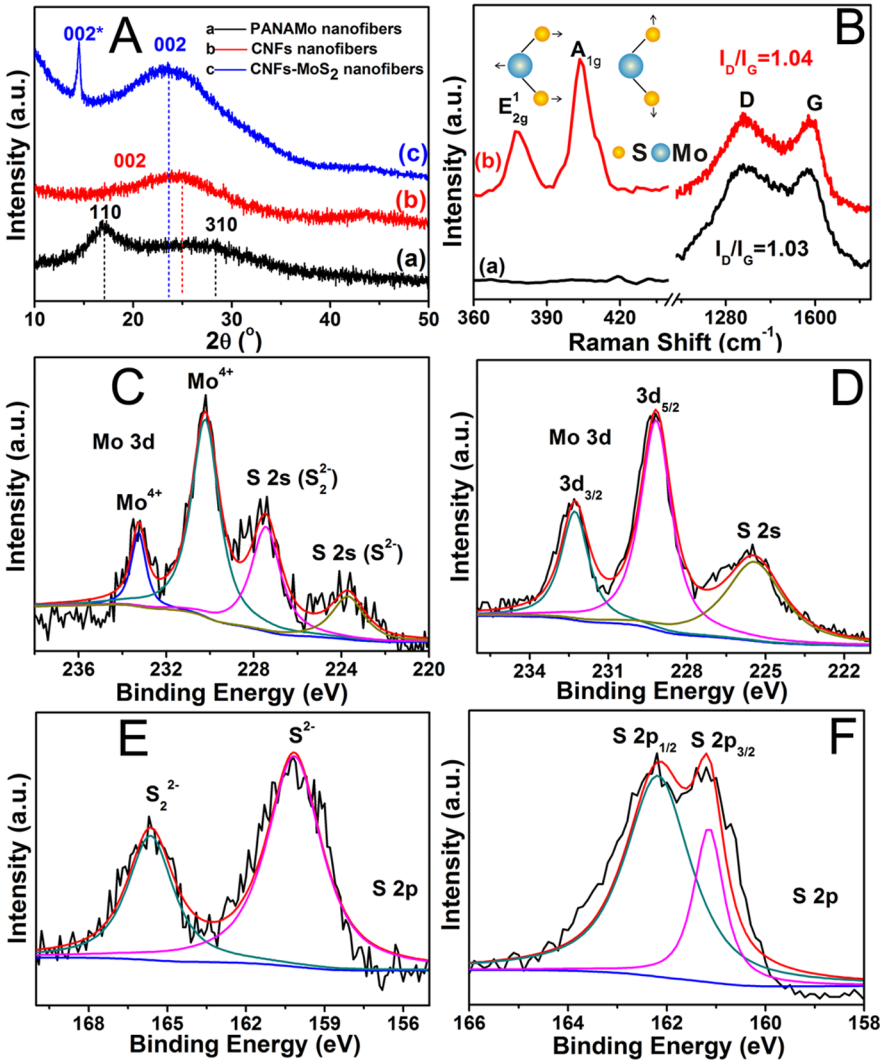

Figure 3. (A) XRD patterns of the (a) PANAMo, (b) pure CNFs, and (c) MoS_2−CNFs nanofibrous mats. (B) Raman spectra of the (a) pure CNFs and (b) MoS_2−CNFs nanofibrous mats. Mo 2d XPS spectra of (C) PANAMo and (D) MoS_2−CNFs nanofibrous mats. S 2p XPS spectra of (E) PANAMo and (F) MoS_2−CNFs nanofibrous mats.

PANAMo exhibit a sharp peak at 17.1° and a broad band at 27.5°, which are ascribed to the (110) and (310) planes of PAN crystalline.[43] Meanwhile, pure CNFs display a single diffraction peak, representative of the (002) plane of stacked graphite layers at 2θ = 24.7° (JCPDS 75-1621), indicating the presence of crystalline graphitic carbon in the nanofibers.[45] The relatively broad band in the XRD pattern of MoS_2−CNFs arises from the (002) plane of the graphene layers in the CNFs. In addition, a strong and sharp diffraction peak can be seen at 14.5°, corresponding to the (002) plane of single-phase, hexagonally structured MoS_2 (JCPDS 37-1492).[45]

As the only peaks observable in the spectra of both CNFs and MoS_2−CNFs can be ascribed to the (002) plane, it can be concluded that these planes constitute the majority of exposed surfaces in these samples. This observation is consistent with the above results of the TEM and HAADF-STEM investigations. As described in the literature, hexagonal structures of MoS_2 have three characteristic reflection peaks, centered at approximately 2θ = 14.5°, 33.8°, and 57.1° and corresponding to the (002), (100), and (110) planes, respectively.[2,20,45−47] No (100) and (110) planes were detected in the XRD spectrum of MoS_2−CNFs (Figure 3A, curve c). This is because that the incorporation of MoS_2 nanoplates into the layers of the CNFs considerably restricts the growth and aggregation of MoS_2 layers during the graphitization process, leading to the formation of few-layered MoS_2 nanoplates with poor crystallinity. Using HRTEM (Figure 2d), only the exposed (002) planes can be seen clearly, with no observable (100) and (110) planes.

The Raman analysis shown in Figure 3B also confirms the formation of a pure MoS_2 phase within the CNFs. The spectrum of nanofibrous mats composed purely of CNFs displays two bands at 1345 and 1578 cm^{-1}, corresponding to the D and G bands.[33,41] Apart from these signals, the MoS_2−CNFs hybrid nanomaterials also exhibit two sharp peaks located at 380.1 and 403.2 cm^{-1}, which are associated with the in-plane E^1_{2g} and out-of-plane A^1_g vibrational modes of hexagonal MoS_2.[2,33] Previous research efforts have reported that information concerning the nature of the MoS_2 crystal termination can be deduced from the relative integrated intensities of these peaks. A relatively greater intensity of the A^1_g mode compared to the E^1_{2g} mode indicates the formation of an edge-terminated structure, while the converse is correlated with terrace surface-termination.[2] In this inves-

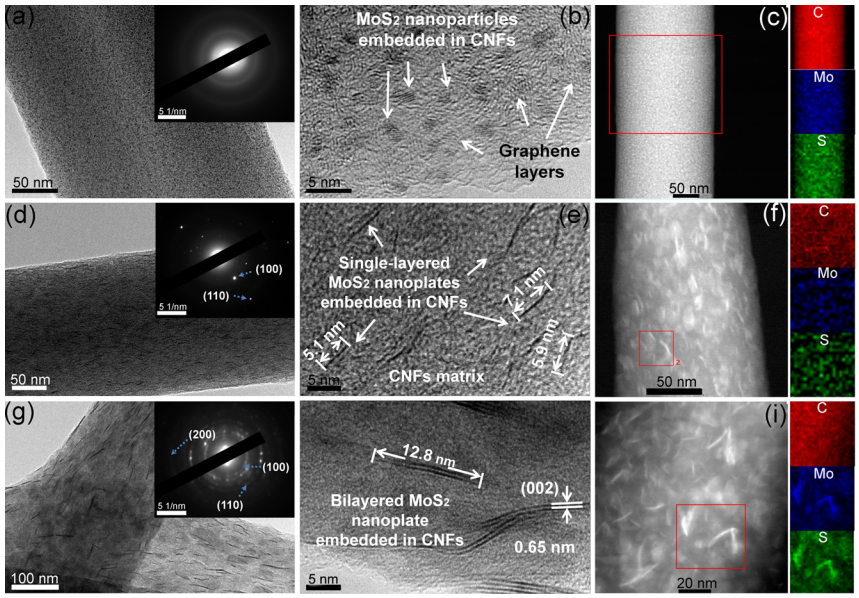

Figure 4. TEM, HRTEM, HAADF-STEM, and STEM-EDS mapping images of the MoS_2−CNFs nanofibers prepared under different graphitization temperatures: (a−c) 900, (d−f) 1000 and (g−i) 1100 °C. Insets in panels a, d, and g are the selected area electron diffraction (SAED) patterns of the MoS_2−CNFs. All MoS_2−CNFs nanofibers had a $(NH_4)_2MoS_4$ mass fraction of 12 wt % and were treated at 2 °C/min.

tigation, the intensity of the A^1_g peak is greater in the Raman spectrum of the MoS_2−CNFs, indicating that the as-prepared MoS_2 structures are edge-terminated. This edge termination appears to increase the amount of exposed edge sites.

The PANAMo and MoS_2−CNFs nanofibrous mats were characterized using X-ray photoelectron spectroscopy (XPS) in order to better describe the formation of MoS_2 nanoplates. As shown in Figure S1 (Supporting Information), the C 1s spectrum of pure PANAMo nanofibers may be deconvoluted into three characteristic subpeaks, located at 285.1, 286.3, and 286.9 eV. These subpeaks are assigned to C—C, C≡N and C═O groups, respectively.[33,41] For pure CNFs (Figure S1, Supporting Information), the C 1s spectrum exhibits four characteristic subpeaks located at 284.9, 286.1, 287.6, and 290.6 eV, which correspond to graphitized carbon, carbon in phenolic or C═O groups, carbon in carbonyl or quinine groups, and carbon in adsorbed CO and CO_2. These results are in agreement with previous studies of PAN-based carbon nanofibers.[33,41] For MoS_2−CNFs (Figure S2, Supporting Information), the binding energy (BE) of C═C/C—C bonds (284.4 eV) is downshifted by ∼0.5 eV compared to that of pure CNFs (284.9 eV), indicating a significant amount of charge transfer from CNFs to the MoS_2 nanoplates, which may improve both the current density and catalytic activity of the resulting hybrid material.[2,48]

The Mo 3d XPS spectrum of PANAMo nanofibers (Figure 3C) contains four distinct peaks, located at 233.3, 230.2, 227.5, and 223.8 eV and corresponding to the Mo 3d and S 2s of $(NH_4)_2MoS_4$. The Mo 3d doublet, with peaks at 233.3 and 230.2 eV, is assigned to the Mo $3d_{3/2}$ and Mo $3d_{5/2}$ of Mo(IV) ions.[2] The S 2s peaks at 227.5 and 223.8 eV are attributed to bridging S_2^{2-} and S^{2-} species, indicating that $(NH_4)_2MoS_4$ exists in two chemical states. In addition, in the S 2p spectrum (Figure 3E), there is a doublet located at BEs of 165.6 and 160.2 eV, which also corresponds to the S species in $(NH_4)_2MoS_4$, including disulfides (S_2^{2-}) as well as S^{2-} ligands.[2,48,49] The Mo 3d spectrum of MoS_2−CNFs (Figure 3D) shows two peaks at 232.2 and 229.2 eV, which are due to the doublet Mo $3d_{3/2}$ and Mo $3d_{5/2}$ orbitals and are characteristic peaks of MoS_2. Notably, the BEs of the Mo 3d peaks shift from 233.3 and 230.2 eV in the spectrum of the PANAMo nanofibers to 232.2 and 229.2 eV in the MoS_2−CNF nanofiber spectrum, adding further evidence of the formation of MoS_2 nanoplates during the graphitization process. The MoS_2−CNFs S 2p spectrum can be deconvoluted into two peaks located at 162.2 and 161.2 eV, which represent the S $2p_{1/2}$ and S $2p_{3/2}$ orbitals of divalent sulfide ions (S^{2-}). These values are consistent with those previously reported for MoS_2 nanocrystals.[2,33,50] High BE of S species, with associated peaks between 168 and 170 eV, were not detected, indicating that only pure MoS_2 is present, with no oxidized phase.

To investigate the temperature dependence of the thermosensitive morphology of the samples, a series of graphitizations were performed at temperatures from 900 to 1100 °C. All samples were imaged using TEM, HRTEM, HAADF-STEM, and STEM-EDS mapping. Figure 4a−c shows the MoS_2−CNF nanofibers prepared at 900 °C. Quasi-spherical MoS_2 nanoparticles with an average diameter of 1.3 nm are evenly dispersed throughout the CNF matrix. Figure 4b indicates that the MoS_2 nanoparticles are surrounded by the graphene layers while the SAED pattern displays only randomly oriented CNF polycrystallites without any MoS_2 diffraction spots, suggesting the low crystallinity of the MoS_2 nanoparticles. HAADF-STEM images of MoS_2−CNFs also show that the MoS_2 nanoparticles (seen as white spots) are well-dispersed. The distribution of C, Mo, and S seen in STEM-EDS mapping images of a selected area further demonstrates the formation of MoS_2 nanoparticles.

As expected, small and uniform MoS_2 nanoplates were formed in the CNF matrix after treatment at 1000 °C (Figure 4d). A HRTEM image (Figure 4e) reveals single-layer MoS_2 nanoplates randomly embedded in the CNFs. The lateral dimension of these nanoplates is only 5.9 ± 4.1 nm, which is exciting not only because of the extremely short perpendicular distance it represents but also because it implies a very small lateral transport length and extreme confinement of the local

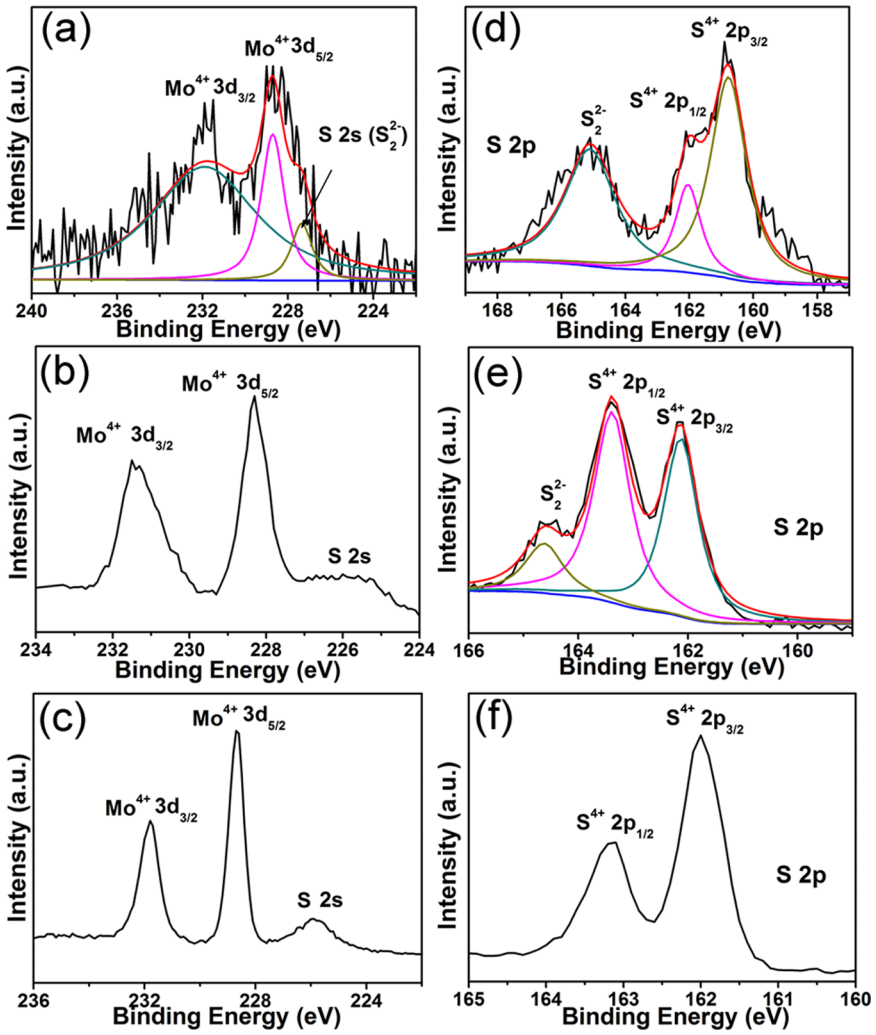

Figure 5. XPS of Mo 3d (a–c) and S 2p (d–f) of the MoS_2–CNFs nanofibers prepared under different graphitization temperatures at (a, d) 900, (b, e) 1000, and (c, f) 1100 °C.

electroactive mass. This latter point is crucial to the reversibility of "conversion" reactions. Figure 4f also clearly shows that the MoS_2 nanoplates are uniformly dispersed throughout the CNF matrix. Similar results may be observed in the STEM-EDS mapping images, wherein the selected area is full of C, Mo, and S signals. When the annealing temperature was increased to 1100 °C, the formerly small MoS_2 nanoplates grew to larger sizes (Figure 4g). A typical two-layer MoS_2 nanoplate structure with an interlayer spacing of 0.65 nm can be observed in Figure 4h. The lateral dimension of the nanoplates increased to 12.8 nm. Figure 4i contains strong signals from the larger MoS_2 nanoplates, with STEM-EDS mapping images displaying a distribution of Mo and S that is consistent with the edge morphology of MoS_2 nanoplates, demonstrating an increase in the number of MoS_2 layers.

XPS analysis was used to further investigate the evolution of sample morphology and the XPS results are summarized in Table S1 (Supporting Information). Figure 5a shows the Mo 3d spectrum of MoS_2 nanoparticles–CNFs graphitized at 900 °C. The binding energies of the Mo $3d_{5/2}$ and Mo $3d_{3/2}$ peaks, 228.7 and 231.8 eV, are characteristic of MoS_2. A small S 2s peak is visible as well, corresponding to polysulfides or bridging S_2^{2-}. In the S 2p spectrum (Figure 5d), the main doublet (located at 160.8 and 162.1 eV) corresponds to the S $2p_{3/2}$ and S $2p_{1/2}$ orbitals of MoS_2. In addition, there is a peak located at a higher BE, 165.4 eV, which arises from bridging S_2^{2-} and/or apical S^{2-}. The ratio of S to Mo in MoS_2 nanoparticle–CNF hybrids prepared at 900 °C is calculated to be 2.66:1 (Table S1, Supporting Information), indicating the formation of S-rich MoS_2 nanostructures. In the spectra collected from a sample of MoS_2 nanoplate–CNFs graphitized at 1000 °C, the Mo 3d scan has two distinct peaks at 228.5 and 231.7 eV, which can be assigned to doublet Mo $3d_{5/2}$ and Mo $3d_{3/2}$, respectively (Figure 5b). The S 2p scan exhibits three peaks located at 164.5, 163.4, and 162.1 eV, which are due to bridging S_2^{2-} and/or apical S^{2-}, and the S $2p_{1/2}$ and S $2p_{3/2}$ orbitals of divalent sulfide ions (S^{2-}) (Figure 5e).

The results from the Mo and S scans are in good agreement with the existence of layered MoS_2 structures. Bridging S_2^{2-} and/or apical S^{2-} species can be detected in MoS_2 nanoplate–CNFs. The ratio of S to Mo in MoS_2 nanoplate-CNF samples treated at 1000 °C is calculated to be 2.33:1 (Table S1, Supporting Information), suggesting the formation of S-rich, layered MoS_2 structures. Similarly, the Mo 3d scan of samples graphitized at 1100 °C shows the doublet Mo $3d_{5/2}$ and Mo $3d_{3/2}$ orbitals at 228.7 and 231.8 eV and S 2s at 225.9 eV, respectively, confirming the formation of a layered structure. In addition, the observed peaks at 163.1 and 162.0 eV correspond

dx.doi.org/10.1021/am505544g | ACS Appl. Mater. Interfaces 2014, 6, 22126–22137

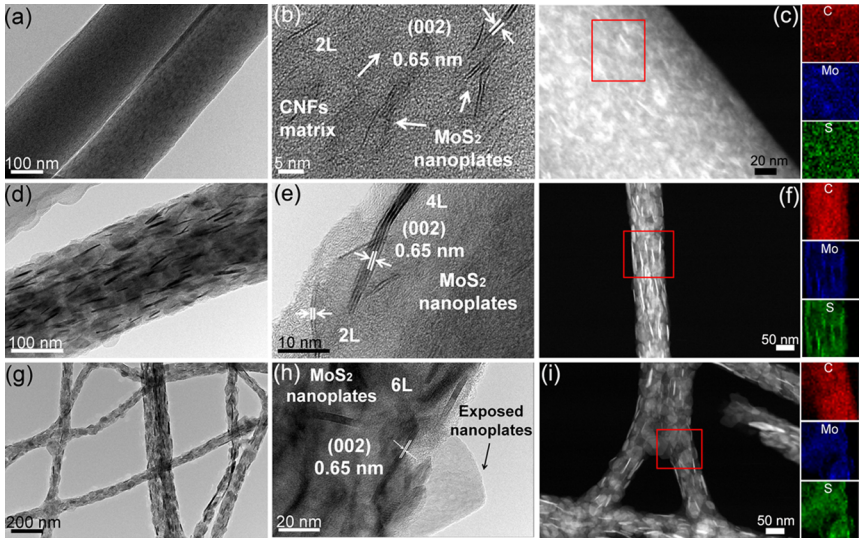

Figure 6. TEM, HRTEM, HAADF-STEM, and STEM-EDS mapping images of the MoS_2−CNFs nanofibers obtained at different heating rates: (a−c) 5, (d−f) 10 and (g−i) 15 °C/min. All the products were prepared at 1000 °C using a $(NH_4)_2MoS_4$ mass fraction of 15 wt %. The selected areas marked as red frame are the mapping areas.

Table 1. Statistics of the MoS_2−CNFs Hybrid with Different Mass Fraction of $(NH_4)_2MoS_4$ Treated at Different Heating Rates

samples	lateral dimension (nm)	number of layers	average diameter of the nanofibers (nm)	heating rates (°C/min)	mass fraction of $(NH_4)_2MoS_4$ (%)
MoS_2−CNFs-5-1	12.6 ± 5.4	2	270 ± 40	5	5
MoS_2−CNFs-5-2	22.3 ± 2.1	2	265 ± 42	10	5
MoS_2−CNFs-5-3	43.1 ± 6.5	2	261 ± 38	15	5
MoS_2−CNFs-10-1	13.3 ± 4.6	2	215 ± 36	5	10
MoS_2−CNFs-10-2	28.6 ± 5.1	2	220 ± 38	10	10
MoS_2−CNFs-10-3	46.6 ± 6.4	3 to 5	208 ± 40	15	10
MoS_2−CNFs-10-1	7.3 ± 2.5	1 to 2	130 ± 25	5	15
MoS_2−CNFs-10-2	31.2 ± 4.6	2 to 4	125 ± 22	10	15
MoS_2−CNFs-10-3	66.7 ± 9.5	6	120 ± 20	15	15

to the S $2p_{1/2}$ and S $2p_{3/2}$ orbitals of divalent sulfide ions (S^{2-}). However, there are no peaks corresponding to bridging S_2^{2-} species detected for MoS_2 nanoplate-CNFs prepared at 1100 °C, and the ratio of S to Mo was found to be only 2.02:1 (Table S1, Supporting Information), indicating that annealing at higher temperatures produces a higher purity MoS_2 phase.

During low-temperature graphitization (below 400 °C), the $(NH_4)_2MoS_4$ decomposes to MoS_3, forming MoS_3−CNFs. Upon increasing the temperature (above 800 °C), the as-formed MoS_3 begins to be converted to MoS_2. Above 800 °C, graphene layers are formed in the CNFs, confining the growth of MoS_2 structures. The conversion from MoS_3 to MoS_2 depends strongly on the graphitization temperature, with higher temperatures leading to increasingly vigorous molecular motion. At elevated temperatures, more MoS_2 nuclei are generated and undergo more collisions with one another, leading to the formation of larger MoS_2 crystals. This trend results in an evolution from nanoparticles to layered nanoplates.

The experiments described above show an evolution in MoS_2 morphology from nanoparticles to layered structures with increasing temperature and all tests were performed on samples that had been treated with a heating rate of 2 °C/min. Higher heating rates have been shown to lead to significant shrinkage of the CNFs and more rapid conversion from MoS_3 to MoS_2.[41] As such, samples with three different $(NH_4)_2MoS_4$ mass fractions (5, 10, and 15 wt %) were heated at different rates to a graphitization temperature of 1000 °C in order to explore the influence of heating rate on the thermally sensitive morphological evolution. Figures S3 and S4 (Supporting Information) show MoS_2−CNFs prepared at heating rates ranging from 5 to 15 °C/min from a starting material with 5 and 10 wt % of $(NH_4)_2MoS_4$. They both exhibit a significant trend that an increase in the heating rate leads to increases in both the lateral dimension and numbers of layers of MoS_2 nanoplates. More discussion can be found in the Supporting Information.

The results for samples prepared using the highest mass ratio, 15%, can be found in Figure 6. For these samples, the evolution of nanoplate morphology depends strongly on heating rate. As shown in Figure 6a,b (5 °C/min), small MoS_2 nanoplates are generated in a random distribution within the CNFs. The nanoplates have one or two layers and a lateral dimension of approximately 7.3 ± 2.5 nm. The shapes and faces of the larger hexagonal MoS_2 nanoplates can be observed clearly in Figure 6c. Because of the higher mass fraction used in the starting material, MoS_2 nanoplates are close-packed and fill much of the volume of the CNFs.

As expected, a higher heating rate (10 °C/min) leads to the formation of larger MoS_2 nanoplates (Figure 6d,e). The majority of these nanoplates have four layers, but there is also a portion of smaller nanoplates with bilayer structures. The lateral dimension of these plates is 31.2 ± 4.6 nm and the STEM-EDS mapping images confirmed the formation of MoS_2. However, when a heating rate of 15 °C/min is used, the hybrid

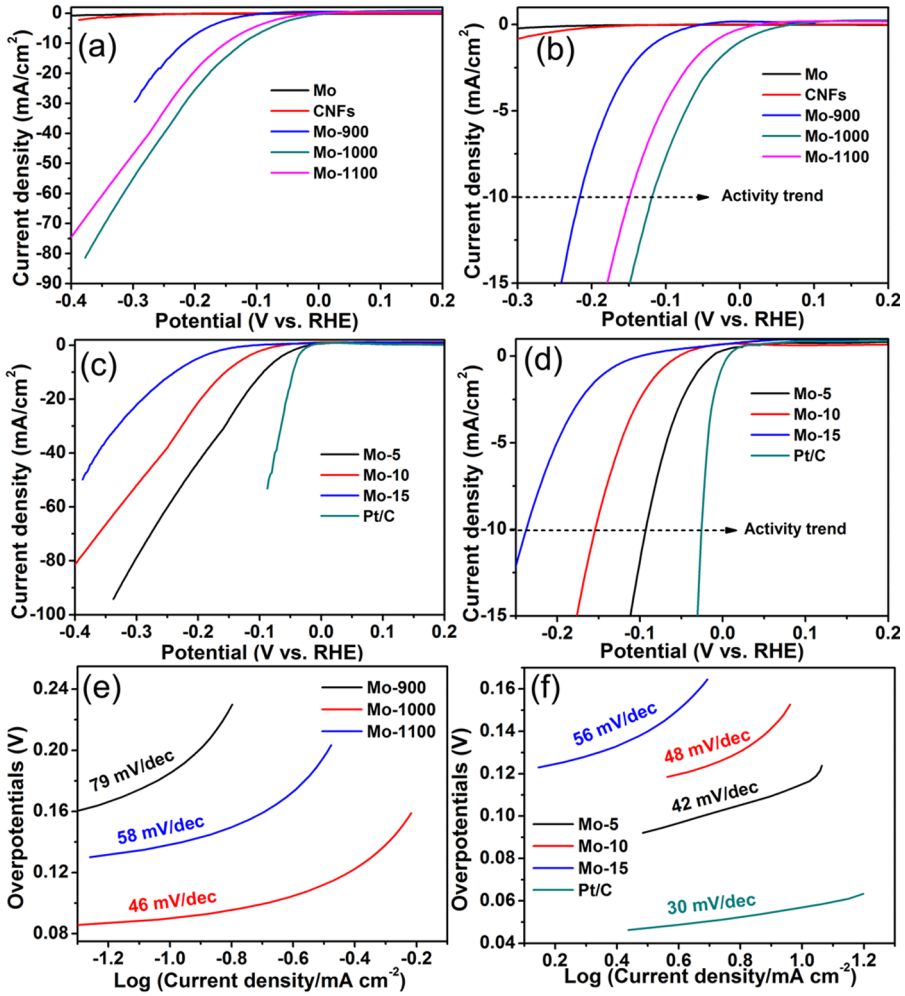

Figure 7. Polarization curves, enlargement of the onset region and the corresponding Tafel plots of MoS_2−CNFs hybrids treated at different (a, b, and e) graphitization temperatures and (c, d, and f) heating rates.

nanofibers undergo a remarkable amount of shrinkage, with the large MoS_2 nanoplates becoming ejected from the CNFs. The average diameter of the CNFs decreases significantly to 130 nm while the lateral dimension of the plates increases to 66.7 ± 9.5 nm. The numbers of layers in the plates increases as well, to 6. Figure 6i exhibits carbon from the CNFs (shown in red) as well as Mo and S signals in an arrangement that is consistent with hexagonal nanoplate morphology.

XRD analysis further corroborates the existence of these evolutions, as shown in Figure S5 (Supporting Information). It is clear from all investigations that the sizes, number of layers, and morphology of the MoS_2 structures formed during graphitization strongly depend on heating rates. The properties of MoS_2−CNF hybrids treated at different conditions are shown in Table 1. For samples prepared using the same initial composition but increasing heating rates, MoS_2 nanoplates grow from small, thin, irregular single- or bilayer nanoplates to large, uniform, multilayer hexagonal structures. However, when a low heating rate (5 °C/min) is maintained, MoS_2 nanoplates develop only one or two layers regardless of mass fraction. Increasing the heating rate to a higher level (10 or 15 °C/min), significant dimensional growth is produced. Raising the graphitization temperature and the heating rate leads to vigorous molecular motion and an increase in the collisions of as-formed MoS_2 molecules, the conversion from MoS_3 to MoS_2 and leading to the formation of larger MoS_2 nanoplates.

These novel MoS_2−CNF hybrid nanomaterials may be used as highly efficient electrocatalysts for the HER. To investigate morphology-dependent catalytic properties, electrochemical measurements (Figure 7) were collected of the HER activity of MoS_2−CNFs nanohybrids prepared using different graphitization conditions, as well as of bulk CNFs, MoS_2, and commercial Pt/C catalysts. All measurements were carried out at an optimized catalyst loading weight of 0.280 mg cm^{-2}. The electrochemical parameters of all MoS_2−CNF hybrid nanomaterials are summarized in Table 2. In these experiments, MoS_2−CNFs treated at 900, 1000, and 1100 °C (5 °C/min) are referred to as Mo-900, Mo-1000, and Mo-1100, respectively, whereas bulk MoS_2 is abbreviated as Mo. The morphology of the hybrid nanomaterial samples was the same as that shown in Figure 4.

As shown in Figure 7, polarization curves of the current density (J) plotted against potential show the HER activity of the Mo-900, Mo-1000, and Mo-1100 in comparison with pure CNFs, MoS_2. Pure MoS_2 exhibits the onset of HER activity near −250 mV vs reversible hydrogen electrode (RHE), consistent with previous reports.[5,31] The Mo-900 displays improved HER activity, and the onset of the catalytic activity shifts to a relatively lower overpotential, as significant H_2

Table 2. Electrochemical Parameters of the MoS_2−CNFs Hybrid Electrocatalysts

samples	current density at η = 300 mV (mA/cm^2)	Overpotentials at current density of 10 mA/cm^2 (mV)	Tafel slopes (mV/decade)	charge-transfer resistance, R_{ct}/Ω
Mo-900	29.6	215	79	267
Mo-1000	54.9	120	46	118
Mo-1100	47.8	148	58	254
Mo-5	80.3	93	42	47
Mo-10	51.1	155	48	64
Mo-15	22.5	238	56	425

evolution (J = 10 mA/cm^2) is observed at a voltage as low as −215 mV (Figure 7b). Meanwhile, the Mo-1000 and Mo-1100 show dramatically lower overpotentials, as significant H_2 evolution (J = 10 mA/cm^2) is observed at a voltage as low as −120 and −148 mV (Figure 7b). It suggests that the single-layer MoS_2 nanoplates (Mo-1000) are more catalytically active than MoS_2 NPs (Mo-900) or large bilayer MoS_2 nanoplates (Mo-1100). Figure 7b clearly reflects the trend in activity.

The effect on HER activity of the morphological differences brought about by differences in heating rate was also investigated by comparing MoS_2−CNFs (15 wt %, 1000 °C) treated using heating rates of 5, 10, and 15 °C/min. These samples are referred to as Mo-5, Mo-10, and Mo-15, and have the morphologies shown in Figures 6. All the three samples exhibit much lower overpotential, as significant H_2 evolution (J = 10 mA/cm^2) is observed at a voltage as low as −238, +155, and +93 mV (Figure 7d). The single-layer Mo-5 sample demonstrates the lowest HER overpotential of all samples, at 93 mV (J = 10 mA/cm^2). With the application of increasingly negative potential, the cathodic current rises rapidly in a pattern that is close to that of commercial Pt/C catalysts. The cathodic current density shown by sample Mo-5, 80.3 mA/cm^2 at η = 300 mV, is much higher than those of samples Mo-10 and Mo-15, at 51.1 and 22.5 mA/cm^2 respectively, indicating that single- and bilayer MoS_2 nanoplates yield superior HER activity. The HER overpotential demonstrated with these catalysts is superior to most reported values for MoS_2-based catalysts, which are typically over 150 mV.[2,5,51] This suggests that small, thin MoS_2 nanoplates with single- or bilayer structures and abundant exposed edges offer better HER activity than other MoS_2 morphologies. As increased heating rates lead to increases in the lateral dimension and number of layers, they result in a decrease in HER activity. Recently, Yu et al. have confirmed that increased layers of MoS_2 nanosheets would affect the HER activity, resulting in a significant decrease.[52] Previous reports have confirmed that HER activity is localized on the sulfur edges of MoS_2 plates, while the basal planes of such plates are catalytically inert.[1,2,6] As such, nanoscale MoS_2 with extensive exposed edge sites should produce more HER activity than bulk materials. This prediction is borne out by the results above, which show that small, thin MoS_2 nanoplates with single-layer or bilayer structures have abundant sulfur edge sites, leading to greater HER activity. In addition, increases in the number of layers and lateral dimension lead to a decrease in the available active edges and increases in the local electroactive mass, resulting in poor HER activity.

The Tafel slope is an inherent property of electrocatalysts and is determined by the rate-limiting step of the HER.[5,51] When the Volmer reaction is the rate-limiting step of the HER, a slope of 120 mV/decade should be observed, whereas if the Heyrovsky or Tafel reaction acts as the rate-limiting step, a Tafel slope of 30 mV/decade or 40 mV/decade, respectively, is measured. For a complete HER process that produces molecular hydrogen, a combination of steps, i.e., Volmer−Heyrovsky or Volmer−Tafel mechanism, is required.

In this investigation, MoS_2 nanoparticles and large MoS_2 nanoplates (samples Mo-900, Mo-1100, and Mo-1000) were found to exhibit Tafel slopes of 79, 58, and 46 mV/decade (Figure 7e). In addition, the observed Tafel slopes of 56, 48, and 42 mV/decade for Mo-15, Mo-10, and Mo-5 are nearly the smallest measured to date for a MoS_2-based catalyst, suggesting that the Volmer−Heyrovsky HER mechanism is operative during the HER as catalyzed by these samples.[2,5,51] It is commonly postulated that a small Tafel slope will lead to significant enhancement of the HER rate with only a moderate increase in the overpotential, a property that is beneficial in practical applications.

The excellent HER performance of the catalysts prepared here can be ascribed to their advantageous morphology of ultrathin nanoplates with abundant accessible edges, as well as to the favorable chemical and electronic coupling between the MoS_2 nanoplates and the CNF. Strong chemical couplings lead to confined growth of the highly dispersed MoS_2 nanoplates. This situation results in small, ultrathin, highly dispersed MoS_2 nanoplates, thereby providing an abundance of accessible edges that may serve as active catalytic sites for the HER. Meanwhile, the CNF matrix also form an interconnected, conductive network and electrical coupling between the MoS_2 structures and the graphene therefore allows rapid electron transport from the less-conductive MoS_2 to the electrodes.

Electrochemical impedance spectroscopy (EIS) was performed at an overpotential of η = 0.3 V to investigate the electrode kinetics and interface reactions undergone by the MoS_2−CNF hybrids during the HER process (Figure S6, Supporting Information). Table 2 contains impedance parameters that were obtained by fitting the electrochemical impedance spectroscopy (EIS) response. Sample Mo-1000 demonstrates the lowest charge transfer resistance (R_{ct}), 118 Ω, indicating that this sample offers the fastest HER kinetics. The R_{ct} of the MoS_2−CNFs prepared at different graphitization temperatures increases in the sequence Mo-1000 < Mo-1100 < Mo-900, which is in agreement with the HER results above (Figure 7a). Bulk MoS_2 and pure CNFs, which were used as controls, show negligible HER activities due to their lack of conductivity (for MoS_2) or activity (for the CNFs). Changing the heating rate also lead to an effect on R_{ct}, which decreases to 425 Ω for sample Mo-15 to 47 Ω for sample Mo-5 (Figure S6, Supporting Information), reinforcing the conclusion that the aforementioned chemical and electronic couplings are critical to achieving strong HER activity. Samples Mo-1000, Mo-5, and Mo-10 share a small, ultrathin morphology with abundant accessible edges as well as exhibiting the lowest R_{ct}, demonstrating that HER activity is morphology-dependent HER.

When compared with the R_{ct} of bulk MoS_2 ($Z_f \approx 10$ kΩ) and pure CNFs ($Z_f \approx 1$ kΩ), the low R_{ct} values measured using MoS_2−CNF hybrid materials suggest that these samples' enhanced electrocatalytic performance originates not only from the increase in electrical conductivity due to the use of conductive CNFs but rather from a complex interaction between the CNFs and MoS_2 nanoplates that synergistically

promotes the HER. The XPS results shown in Figures S1 and S2 (Supporting Information) also corroborate the existence of strong electron transport between the CNFs and MoS_2. For MoS_2−CNFs (Figure S2, Supporting Information), the BE of C═C/C—C bonds (284.4 eV) is downshifted by about 0.6 eV compared to that of pristine CNFs (285.0 eV), indicating a significant amount of charge transfer from CNFs to the MoS_2 nanoplates, which improves both the current density and catalytic activity of the resulting hybrid material.[2,48]

In addition to catalytic activity, stability is also an important property to consider when evaluating an advanced electrocatalyst. The stability of sample Mo-5, which exhibited among the best HER activities, was investigated by continuous cycling for 1000 cycles in an acidic environment. As shown in Figure S7 (Supporting Information), almost no difference can be observed between the initial and final curves, demonstrating that this sample possesses excellent durability during long-term cycling. Both the high activity offered by this optimized catalyst as well as its impressive stability can be attributed to the following two aspects: (i) small, ultrathin, mono- or bilayer MoS_2 nanoplates offer large quantities of unsaturated sulfur atoms to serve as active sites for hydrogen evolution; (ii) chemical coupling and the concomitant redistribution of electron between the CNFs and the MoS_2 provides a negligible-resistance path for fast electron transfer, thereby accelerating the kinetics of the HER as catalyzed on the MoS_2 surface. This finding may provide a general strategy for the synthesis of other 2D transition metal sulfide-based catalysts, such as WS_2 and TeS_2, thereby paving the way for performance-oriented molecular design of these novel materials.

CONCLUSION

A new schema has been proposed for the synthesis of small, ultrathin, 2D MoS_2 nanoplates with abundant active edges within 1D carbon nanofibers. This strategy allows the formation of favorable nanosized products with monolayer thicknesses, nanoscale lateral, and abundant edges. The use of CNFs provides both an electronic mediator and substrate and a host matrix to confine the growth of the MoS_2 nanoplates, increasing the exposure of edge sites and hindering the stacking and aggregation of MoS_2 layers. It has been conclusively shown that the MoS_2 nanocrystals have thermosensitive morphologies, leading to intriguing phenomena. As the graphitization temperature is increased from 900 to 1100 °C, the morphology of the MoS_2 nanocrystals shifts from nanoparticles to nanoplates, and both the lateral dimension and the number of layers increases. Similarly, the use of increased heating rates leads to increases in the lateral dimension from 5 to 70 nm, while the number of layers increases from 1 to 6. Moreover, a phase transition from 1T MoS_2 to 2H MoS_2 is observed as the heating rate is increased. Single-layered MoS_2 nanoplates with a lateral dimension of 7.3 nm demonstrated the lowest HER overpotential of all samples, at 93 mV (J = 10 mA/cm^2), which is very close to the value shown by commercial Pt/C catalysts. These samples produced the highest current density, 80.3 mA/cm^2 at η = 300 mV, and the smallest Tafel slope, 42 mV/decade, indicating that the Volmer−Heyrovsky mechanism acts as the rate-limiting step for this catalyst. MoS_2−CNF hybrid nanomaterials are able to act as nonprecious metal catalysts, suggesting that they have a promising future in energy-related electrocatalytic applications.

EXPERIMENTAL SECTION

Synthesis of Small MoS_2 Nanoplates Embedded in Carbon Nanofibers. In a typical procedure, 3.000 g of polyacrylonitrile (PAN) powder was dissolved in 22 mL of dimethylformamide (DMF) under magnetic stirring at 65 °C to get a homogeneous solution with a mass ration of 12 wt %. Then, 0.1000 g of $(NH_4)_2MoS_4$ was added into the PAN/DMF solution and then transferred into a syringe with a stainless copper needle at the tip. The needle was connected to a high voltage power supply. The applied voltage was 12 kV, the needle-to-collector distance was 12 cm, and the flow rate of the solution was 0.6 mL/h. All experiments were performed at room temperature. The as-collected electrospun PANAMo nanofibrous mats were peeled off from the aluminum foil and placed into a home-built chemical vapor deposition (CVD) tube furnace for heat treatment. The PANAMo nanofibrous mats were first heated to 280 °C in air at a rate of 5 °C/min and maintained for 6 h for stabilization, then the samples were heated up to 900 °C at a rate of 5 °C/min under Ar gas flow (150 sccm) for the graphitization. The desired graphitization temperature was held constant for 8 h and then the products were cooled to room temperature under an Ar atmosphere.

Electrochemical Measurements. Electrochemical experiments of the samples were performed on a glassy carbon electrode in 0.5 M H_2SO_4 solution using a typical three-electrode system in which a MoS_2−CNFs fibrous mats electrode, graphite electrode and saturated Ag/AgCl electrode served as the working, counter and reference electrodes, respectively. Four milligrams of catalyst and 80 μL of 5 wt % Nafion solution were dispersed in 1 mL of 4:1 v/v water/ethanol by at least 30 min of sonication to form a homogeneous ink. Then 15 μL of the catalyst ink was loaded onto a glassy carbon electrode (GCE, 5 mm in diameter). The HER activity was evaluated by linear sweep voltammetry conducted with Autolab potentiostat/galvanostat (Model PGSTAT302N) workstation with scan rate of 2 mV s^{-1}. The polarization curves were obtained after *i*R-compensation. In all measurements, we used a Ag/AgCl electrode as the reference and the potential values are corrected to reverse hydrogen electrode (RHE). In 0.5 M H_2SO_4, E(RHE) = E (Ag/AgCl)+0.204 V. Prior to any electrochemical measurement, the electrolyte solution was purified with N_2 for 1 h to remove completely the oxygen, and stable polarization performance was recorded after 10 cycles.

Material Characterizations. Transmission electron microscopy (TEM) images were taken by a JSM-2100 transmission electron microscope (JEOL, Japan) at an acceleration voltage of 200 kV. Field emission scanning electron microscopy (FE-SEM) images were characterized by a JSM-6700F FE-SEM (JEOL, Japan) at an acceleration voltage of 3 kV. X-ray photoelectron spectra of the products were recorded using an X-ray photoelectron spectrometer (Kratos Axis Ultra DLD) with an Al (mono) Kα source (1486.6 eV). The Al Kα source was operated at 15 kV and 10 mA. X-ray diffraction (XRD) patterns were analyzed by a Bruker AXS D8 DISCOVER X-ray diffractometer with Cu Kα radiation (λ = 1.5406 Å) at a scanning rate of 0.02 2θ s^{-1} in the 2θ range of 10−80°. Raman spectra of all the samples were recorded by a RenishawinVia Raman microscope (LabRAM HR800) using a 532 nm laser excitation source. The excitation light intensity in front of the objective was 10 mW with a spectral collection time of 1 s. The integration time for our measurements was set to 10 s. The high-angle annular dark field scanning TEM (HAADF-STEM) image, STEM mapping and line-scan energy dispersive X-ray spectroscopy (EDX) were recorded by a STEM (Tecnai G2 F30S-Twin, Philips-FEI) at an acceleration voltage of 300 kV. The number of layers and lateral dimensional of MoS_2 nanoparticles and nanoplates (200 counts) were measured with Image-Pro Plus 6.2 software.

ASSOCIATED CONTENT

Supporting Information

Assignments of the XPS spectra of PANAMo, pure CNFs nanofibrous and MoS_2−CNFs hybrid, TEM images and XRD patterns of MoS_2−CNFs nanofibers prepared using different heating rates and $(NH_4)_2MoS_4$ mass fraction, Nyquist plots of

the pure MoS_2, CNFs and MoS_2–CNFs hybrid, polarization curve of Mo-5 after 1000 CV cycles. This material is available free of charge via the Internet at http://pubs.acs.org.

AUTHOR INFORMATION

Corresponding Author

*M. Du. E-mail: du@zstu.edu.cn.

Notes

The authors declare no competing financial interest.

ACKNOWLEDGMENTS

This work was supported by the National Natural Science Foundation of China (NSFC) (51373154, 21203137), Zhejiang Top Priority Discipline of Textile Science and Engineering and the 521 Talent Project of Zhejiang Sci-Tech University.

REFERENCES

(1) Jaramillo, T. F.; Jorgensen, K. P.; Bonde, J.; Nielsen, J. H.; Horch, S.; Chorkendorff, I. Identification of Active Edge Sites for Electrochemical H_2 Evolution from MoS_2 Nanocatalysts. *Science* **2007**, *317*, 100–102.

(2) Zheng, X. L.; Xu, J. B.; Yan, K. Y.; Wang, H.; Wang, Z. L.; Yang, S. H. Space-Confined Growth of MoS_2 Nanosheets within Graphite: The Layered Hybrid of MoS_2 and Graphene as an Active Catalyst for Hydrogen Evolution Reaction. *Chem. Mater.* **2014**, *26*, 2344–2353.

(3) Vrubel, H.; Merki, D.; Hu, X. L. Hydrogen Evolution Catalyzed by MoS_3 and MoS_2 Particles. *Energy Environ. Sci.* **2012**, *5*, 6136–6144.

(4) Cheng, L.; Huang, W. J.; Gong, Q. F.; Liu, C. H.; Liu, Z.; Li, Y. G.; Dai, H. J. Ultrathin WS_2 Nanoflakes as a High-Performance Electrocatalyst for the Hydrogen Evolution Reaction. *Angew. Chem., Int. Ed.* **2014**, *53*, 7860–7863.

(5) Li, Y. G.; Wang, H. L.; Xie, L. M.; Liang, Y. Y.; Hong, G. S.; Dai, H. J. MoS_2 Nanoparticles Grown on Graphene: An Advanced Catalyst for the Hydrogen Evolution Reaction. *J. Am. Chem. Soc.* **2011**, *133*, 7296–7299.

(6) Kibsgaard, J.; Chen, Z. B.; Reinecke, B. N.; Jaramillo, T. F. Engineering the Surface Structure of MoS_2 to Preferentially Expose Active Edge Sites for Electrocatalysis. *Nat. Mater.* **2012**, *11*, 963–969.

(7) Merki, D.; Hu, X. L. Recent Developments of Molybdenum and Tungsten Sulfides as Hydrogen Evolution Catalysts. *Energy Environ. Sci.* **2011**, *4*, 3878–3888.

(8) Zheng, Y.; Jiao, Y.; Zhu, Y. H.; Li, L. H.; Han, Y.; Chen, Y.; Du, A. J.; Jaroniec, M.; Qiao, S. Z. Hydrogen Evolution by a Metal-Free Electrocatalyst. *Nat. Commun.* **2014**, *5*, 3783–90.

(9) Li, Y. H.; Cao, L. J.; Qiao, L.; Zhou, M.; Yang, Y.; Xiao, P.; Zhang, Y. H. Ni-Co Sulfide Nanowires on Nickel Foam with Ultrahigh Capacitance for Asymmetric Supercapacitors. *J. Mater. Chem. A* **2014**, *2*, 6540–6548.

(10) Laursen, A. B.; Kegnas, S.; Dahla, S.; Chorkendorff, I. Molybdenum Sulfides-Efficient and Viable Materials for Electro- and Photoelectrocatalytic Hydrogen Evolution. *Energy Environ. Sci.* **2012**, *5*, 5577–5591.

(11) Tran, P. D.; Chiam, S. Y.; Boix, P. P.; Ren, Y. S.; Pramana, S.; Fize, J.; Artero, V.; Barber, J. Novel Cobalt/Nickel-Tungsten-Sulfide Catalysts for Electrocatalytic Hydrogen Generation From Water. *Energy Environ. Sci.* **2013**, *6*, 2452–2459.

(12) Gao, M. R.; Lin, Z. Y.; Zhuang, T. T.; Jiang, J.; Xu, Y. F.; Zheng, Y. R.; Yu, S. H. Mixed-Solution Synthesis of Sea Urchin-like NiSe Nanofiber Assemblies as Economical Pt-Free Catalysts for Electrochemical H_2 Production. *J. Mater. Chem.* **2012**, *22*, 13662–13668.

(13) Merki, D.; Vrubel, H.; Rovelli, L.; Fierro, S.; Hu, X. L. Fe, Co, and Ni Ions Promote the Catalytic Activity of Amorphous Molybdenum Sulfide Films for Hydrogen Evolution. *Chem. Sci.* **2012**, *3*, 2515–2525.

(14) Yan, Y.; Xia, B. Y.; Xu, Z. C.; Wang, X. Recent Development of Molybdenum Sulfides as Advanced Electrocatalysts for Hydrogen Evolution Reaction. *ACS Catal.* **2014**, *4*, 1693–1705.

(15) Chen, W. F.; Muckerman, J. T.; Fujita, E. Recent Developments in Transition Metal Carbides and Nitrides as Hydrogen Evolution Electrocatalysts. *Chem. Commun.* **2013**, *49*, 8896–8909.

(16) Hunt, S. T.; Nimmanwudipong, T.; Roman-Leshkov, Y. Engineering Non-sintered, Metal-Terminated Tungsten Carbide Nanoparticles for Catalysis. *Angew. Chem., Int. Ed.* **2014**, *53*, 5131–5136.

(17) Yan, Y.; Xia, B.; Qi, X.; Wang, H. B.; Xu, R.; Wang, J. Y.; Zhang, H.; Wang, X. Nano-Tungsten Carbide Decorated Graphene as Co-catalysts for Enhanced Hydrogen Evolution on Molybdenum Disulfide. *Chem. Commun.* **2013**, *49*, 4884–4886.

(18) Morales-Guio, C. G.; Stern, L. A.; Hu, X. L. Nanostructured Hydrotreating Catalysts for Electrochemical Hydrogen Evolution. *Chem. Soc. Rev.* **2014**, *43*, 6555–6569.

(19) Liu, Q.; Tian, J. Q.; Cui, W.; Jiang, P.; Cheng, N. Y.; Asiri, A. M.; Sun, X. P. Carbon Nanotubes Decorated with CoP Nanocrystals: A Highly Active Non-Noble-Metal Nanohybrid Electrocatalyst for Hydrogen Evolution. *Angew. Chem., Int. Ed.* **2014**, *126*, 6828–6832.

(20) Yan, Y.; Xia, B. Y.; Ge, X. M.; Liu, Z. L.; Wang, J. Y.; Wang, X. Ultrathin MoS_2 Nanoplates with Rich Active Sites as Highly Efficient Catalyst for Hydrogen Evolution. *ACS Appl. Mater. Interfaces* **2013**, *5*, 12794–12798.

(21) Xie, J. F.; Zhang, H.; Li, S.; Wang, R. X.; Sun, X.; Zhou, M.; Zhou, J. F.; Lou, X. W.; Xie, Y. Defect-Rich MoS_2 Ultrathin Nanosheets with Additional Active Edge Sites for Enhanced Electrocatalytic Hydrogen Evolution. *Adv. Mater.* **2013**, *25*, 5807–5813.

(22) Wang, H. T.; Kong, D. S.; Johanes, P.; Cha, J. J.; Zheng, G. Y.; Yan, K.; Liu, N.; Cui, Y. $MoSe_2$ and WSe_2 Nanofilms with Vertically Aligned Molecular Layers on Curved and Rough Surfaces. *Nano Lett.* **2013**, *13*, 3426–3433.

(23) Merki, D.; Fierro, S.; Vrubel, H.; Hu, X. L. Amorphous Molybdenum Sulfide Films as Catalysts for Electrochemical Hydrogen Production in Water. *Chem. Sci.* **2011**, *2*, 1262–1267.

(24) Vrubel, H.; Moehl, T.; Gratzelb, M.; Hu, X. L. Revealing and Accelerating Slow Electron Transport in Amorphous Molybdenum Sulphide Particles for Hydrogen Evolution Reaction. *Chem. Commun.* **2013**, *49*, 8985–8987.

(25) Vrubel, H.; Hu, X. L. Growth and Activation of an Amorphous Molybdenum Sulfide Hydrogen Evolving Catalyst. *ACS Catal.* **2013**, *3*, 2002–2011.

(26) Wang, X. S.; Feng, H. B.; Wu, Y. M.; Jiao, L. Y. Controlled Synthesis of Highly Crystalline MoS_2 Flakes by Chemical Vapor Deposition. *J. Am. Chem. Soc.* **2013**, *135*, 5304–5307.

(27) Chang, K.; Chen, W. X. L-Cysteine-Assisted Synthesis of Layered MoS_2/Graphene Composites with Excellent Electrochemical Performances for Lithium Ion Batteries. *ACS Nano* **2011**, *5*, 4720–4728.

(28) Cao, X. H.; Shi, Y. M.; Shi, W. H.; Rui, X. H.; Yan, Q. Y.; Kong, J.; Zhang, H. Preparation of MoS_2-Coated Three-Dimensional Graphene Networks for High-Performance Anode Material in Lithium-Ion Batteries. *Small* **2013**, *20*, 3433–3438.

(29) Yin, Z. Y.; Li, H.; Li, H.; Jiang, L.; Shi, Y. M.; Sun, Y. H.; Lu, G.; Zhang, Q.; Chen, X. D.; Zhang, H. Single-Layer MoS_2 Phototransistors. *ACS Nano* **2012**, *6*, 73–80.

(30) Liang, Y. Y.; Li, Y. G.; Wang, H. L.; Dai, H. J. Strongly Coupled Inorganic/Nanocarbon Hybrid Materials for Advanced Electrocatalysis. *J. Am. Chem. Soc.* **2013**, *135*, 2013–2036.

(31) Lukowski, M. A.; Daniel, A. S.; Meng, F.; Forticaux, A.; Li, L. S.; Jin, S. Enhanced Hydrogen Evolution Catalysis from Chemically Exfoliated Metallic MoS_2 Nanosheets. *J. Am. Chem. Soc.* **2013**, *135*, 10274–10277.

(32) Zhu, B. L.; Lin, B. Z.; Zhou, Y.; Sun, P.; Yao, Q. R.; Chen, Y. L.; Gao, B. F. Enhanced Photocatalytic H_2 Evolution On ZnS Loaded With Graphene and MoS_2 Nanosheets as Cocatalysts. *J. Mater. Chem. A* **2014**, *2*, 3819–3827.

(33) Zhu, H.; Du, M. L.; Zhang, M.; Zou, M. L.; Yang, T. T.; Fu, Y. Q.; Yao, J. M. The Design and Construction of 3D Rose-Petal-Shaped

MoS_2 Hierarchical Nanostructures with Structure-Sensitive Properties. *J. Mater. Chem. A* **2014**, *2*, 7680−7685.
(34) Coleman, J. N.; Lotya, M.; O' Neill, A. Two-Dimensional Nanosheets Produced by Liquid Exfoliation of Layered Materials. *Science* **2011**, *331*, 568−571.
(35) Wu, S. X.; Zeng, Z. Y.; He, Q. Y.; Wang, Z. J.; Wang, S. J.; Du, Y. P.; Yin, Z. Y.; Sun, X. P.; Chen, W.; Zhang, H. Electrochemically Reduced Single-Layer MoS_2 Nanosheets: Characterization, Properties, and Sensing Applications. *Small* **2012**, *8*, 2264−2270.
(36) Maitra, U.; Gupta, U.; De, M.; Datta, R.; Govindaraj, A.; Rao, C. N. R. Highly Effective Visible-Light-Induced H_2 Generation by Single-Layer 1T-MoS_2 and a Nanocomposite of Few-Layer 2H-MoS_2 with Heavily Nitrogenated Graphene. *Angew. Chem., Int. Ed.* **2013**, *52*, 13057−13061.
(37) Zhu, C. B.; Mu, X. K.; Aken, P. A. V.; Yu, Y.; Maier, J. Single-Layered Ultrasmall Nanoplates of MoS_2 Embedded in Carbon Nanofibers with Excellent Electrochemical Performance for Lithium and Sodium Storage. *Angew. Chem., Int. Ed.* **2014**, *53*, 2152−2156.
(38) Shi, Y. M.; Wang, Y.; Wong, J. I.; Tan, A. Y. S.; Hsu, C. L.; Li, L. J.; Lu, Y. C.; Yang, H. Y. Self-Assembly of Hierarchical MoS_x/CNT Nanocomposites (2<x<3): Towards High Performance Anode Materials for Lithium Ion Batteries. *Sci. Rep.* **2013**, *3*, 2169−2176.
(39) Shi, Y. M.; Zhou, W.; Lu, A. Y.; Fang, W. J.; Lee, Y. H.; Hsu, A. L.; Kim, S. M.; Kim, K. K.; Yang, H. Y.; Li, L. J.; Idrobo, J. C.; Kong, J. van der Waals Epitaxy of MoS_2 Layers Using Graphene as Growth Templates. *Nano Lett.* **2012**, *12*, 2784−2791.
(40) Wang, T. Y.; Zhuo, J. Q.; Du, K. Z.; Chen, B. B.; Zhu, Z. W.; Shao, Y. H.; Li, M. X. Electrochemically Fabricated Polypyrrole and MoS_x Copolymer Films as a Highly Active Hydrogen Evolution Electrocatalyst. *Adv. Mater.* **2014**, *26*, 3761−3766.
(41) Zhu, H.; Du, M. L.; Zhang, M.; Zou, M. L.; Yang, T. T.; Wang, L. N.; Yao, J. M.; Guo, B. C. Probing the Unexpected Behavior of AuNPs Migrating Through Nanofibers: A New Strategy for the Fabrication of Carbon Nanofiber-Noble Metal Nanocrystal Hybrid Nanostructures. *J. Mater. Chem. A* **2014**, *2*, 11728−11741.
(42) Liu, K. K.; Zhang, W. J.; Lee, Y. H.; Lin, Y. C.; Chang, M. T.; Su, C. Y.; Chang, C. S.; Li, H.; Shi, Y. M.; Zhang, H.; Lai, C. S.; Li, L. J. Growth of Large-Area and Highly Crystalline MoS_2 Thin Layers on Insulating Substrates. *Nano Lett.* **2012**, *12*, 1538−1544.
(43) Zhang, Y. Y.; Song, K. N.; Meng, J. S.; Minus, M. L. Tailoring Polyacrylonitrile Interfacial Morphological Structure by Crystallization in the Presence of Single-Wall Carbon Nanotubes. *ACS Appl. Mater. Interfaces* **2013**, 5807−5814.
(44) Wu, Y. Z.; Reddy, M. V.; Chowdari, B. V. R.; Ramakrishna, S. Long-Term Cycling Studies on Electrospun Carbon Nanofibers as Anode Material for Lithium Ion Batteries. *ACS Appl. Mater. Interfaces* **2013**, *5*, 12175−12184.
(45) Sen, U. K.; Mitra, S. High-Rate and High-Energy-Density Lithium-Ion Battery Anode Containing 2D MoS_2 Nanowall and Cellulose Binder. *ACS Appl. Mater. Interfaces* **2013**, *5*, 1240−1247.
(46) Hwang, H.; Kim, H.; Cho, J. MoS_2 Nanoplates Consisting of Disordered Graphene-like Layers for High Rate Lithium Battery Anode Materials. *Nano Lett.* **2011**, *11*, 4826−4830.
(47) Voiry, D.; Salehi, M.; Silva, R.; Fujita, T.; Chen, M. W.; Asefa, T.; Shenoy, V. B.; Eda, G.; Chhowalla, M. Conducting MoS_2 Nanosheets as Catalysts for Hydrogen Evolution Reaction. *Nano Lett.* **2013**, *13*, 6222−6227.
(48) Koroteev, V. O.; Bulusheva, L. G.; Asanov, I. P.; Shlyakhova, E. V.; Vyalikh, D. V.; Okotrub, A. V. Charge Transfer in the MoS_2/Carbon Nanotube Composite. *J. Phys. Chem. C* **2011**, *115*, 21199−21204.
(49) Lv, X. J.; She, G. W.; Zhou, S. X.; Li, Y. M. Highly Efficient Electrocatalytic Hydrogen Production by Nickel Promoted Molybdenum Sulfie Microspheres Catalysts. *RSC Adv.* **2013**, *3*, 21231−21236.
(50) Park, W.; Baik, J.; Kim, T. Y.; Cho, K.; Hong, W. K.; Shin, H. J.; Lee, T. Photoelectron Spectroscopic Imaging and Device Applications of Large-Area Patternable Single-Layer MoS_2 Synthesized by Chemical Vapor Deposition. *ACS Nano* **2014**, *8*, 4961−4968.
(51) Xie, J. F.; Zhang, J. J.; Li, S.; Grote, F.; Zhang, X. D.; Zhang, H.; Wang, R. X.; Lei, Y.; Pan, B. C.; Xie, Y. Controllable Disorder Engineering in Oxygen-Incorporated MoS_2 Ultrathin Nanosheets for Efficient Hydrogen Evolution. *J. Am. Chem. Soc.* **2013**, *135*, 17881−17888.
(52) Yu, Y. F.; Huang, S. Y.; Li, Y. P.; Steinmann, S. N.; Yang, W. T.; Cao, L. Y. Layer-Dependent Electrocatalysis of MoS_2 for Hydrogen Evolution. *Nano Lett.* **2014**, *14*, 553−558.